J. Membrane Biol. 66, 171–181 (1982)

The Journal of
Membrane Biology

Potassium Currents in the Giant Axon of the Crab *Carcinus maenas*

M. Emilia Quinta-Ferreira, E. Rojas, and N. Arispe*

Department of Biophysics, School of Biological Sciences, University of East Anglia, Norwich NR4 7TJ, England

Summary. Measurements were made of the kinetic and steady-state characteristics of the potassium conductance in the giant axon of the crab *Carcinus maenas*. These measurements were made in the presence of tetrodotoxin, using the feedback amplifier concept introduced by Dodge and Frankenhaeuser (*J. Physiol. (London)* **143**:76–90). The conductance increase during depolarizing voltage-clamp pulses was analyzed assuming that two separate potassium channels exist in these axons. The first potassium channel exhibited activation and fast inactivation gating which could be fitted using the m^3h, Hodgkin-Huxley formalism. The second potassium channel exhibited the standard n^4 Hodgkin-Huxley kinetics. These two postulated channels are blocked by internal application of caesium, tetraethylammonium and sodium ions. External application of 4 amino-pyridine also blocks these channels.

Key words nerve · voltage clamp · giant axon · potassium channels · potassium gating · potassium inactivation

Introduction

In the preceding paper we presented the measurements of the early inward currents in the giant axon of the crab *Carcinus maenas* (Quinta-Ferreira, Arispe & Rojas, 1982). The purpose of this paper is to present the results of experiments designed to study the kinetic and steady-state characteristics of the outward currents in these nerves.

The analysis of the current revealed two distinct components, a fast one, with activation-inactivation kinetics, and a delayed one, similar to the potassium currents recorded in the giant axon of the squid (Hodgkin & Huxley, 1952*b*). These findings confirm and extend previous work by Connor, Walter and McKown (1977) on giant nerve fibers from the crabs *Callinectes sapidus* and *Cancer magister*.

A preliminary report of this work has been presented elsewhere (Arispe, Quinta-Ferreira & Rojas, 1980).

* *Permanent address:* Escuela de Biologia, Universidad Central de Venezuela, Caracas.

Materials and Methods

The feedback amplifier used and the experimental procedures are fully described in the preceding paper (Quinta-Ferreira et al., 1982).

The composition of the solutions used is given in Table 1.

Results

Ionic Currents Recorded with the Fiber in Artificial Seawater

Figure 1 shows two sets of membrane current records made at two different holding potentials, −122 and −92 mV. While the inward currents shown in Fig. 1 are blocked by external application of tetrodotoxin (TTX) the steady-state level of the outward current is not affected. Outward currents in this work were recorded in artificial seawater (ASW) plus TTX at a concentration greater than 100 nM. The outward component of the currents in Fig. 1 is different from that recorded in the giant axon of squid (Hodgkin, Huxley & Katz, 1952). Thus, it may be seen that after 5 msec there is a further increase in the currents which, even after 10 msec, has not reached a steady level.

Figure 2 shows a set of membrane current records made in ASW plus TTX from another experiment. An inspection of each current record reveals that the kinetic is not strictly n^4 (Hodgkin & Huxley, 1952*b*). Thus, following the record at $V_M = -20$ mV during the pulse one can see that there is an initial jump (presumably representing rectification of the leakage current) followed by a fast rise to a maximum value. Thereafter the current record slowly decreases to a minimum level, to increase again towards a steady level. For depolarizing pulses taking the membrane potential towards positive values, a monotonic fast increase in the current is seen.

The experiments described in the following sec-

0022-2631/82/0066-0171 $02.20

Table 1.
A. Internal solutions

Name	|TEA| (mM)	|K^+| (mM)	|Na^+| (mM)	|Cs^+| (mM)	|$TRIS^+$| (mM)	Osmotic pressure (mOsm)
KF-1	–	500	–	–	50	970
KF/NaF	–	350	150	–	5	1030
KF-1 plus TEA	5	500	–	–	50	980
CsF[a]	–	–	–	500	5	1200

B. External solutions

Name	|TTX| (nM)	|K^+| (mM)	|Rb^+| (mM)	|Na^+| (mM)	|Mg^{2+}| (mM)	|Ca^{2+}| (mM)	|$TRIS^+$| (mM)	Osmotic pressure (mOsm)
ASW	–	11	–	470	14	12	5	965
ASW	100	11	–	470	14	12	5	1030
plus TTX	300		–					
High K-SW	300	450	–	–	14	12	10	970

[a] K_2 EGTA was added to a concentration of 1 mM. Also 1% of Dextran. pH of solutions was adjusted to 7.3 ± 0.1. Osmotic pressure was measured using a vapor pressure osmometer.

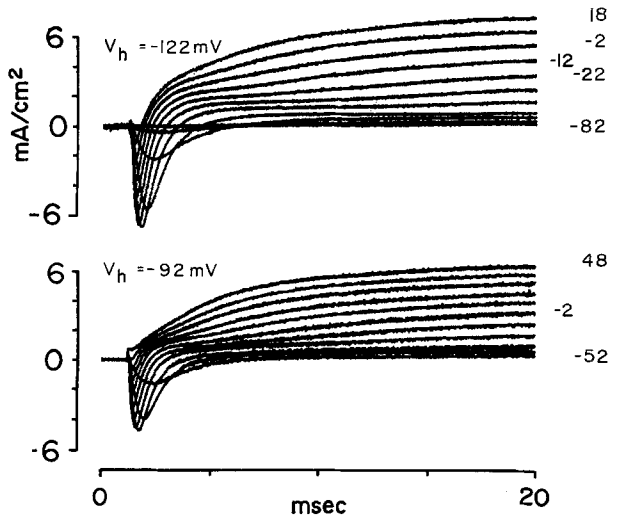

Fig. 1. Inward and outward currents at two different holding potentials. Experiment 790306: fiber in ASW at 17 °C. Cut ends in solution KF-1. Feedback amplifier in the Nonner's configuration

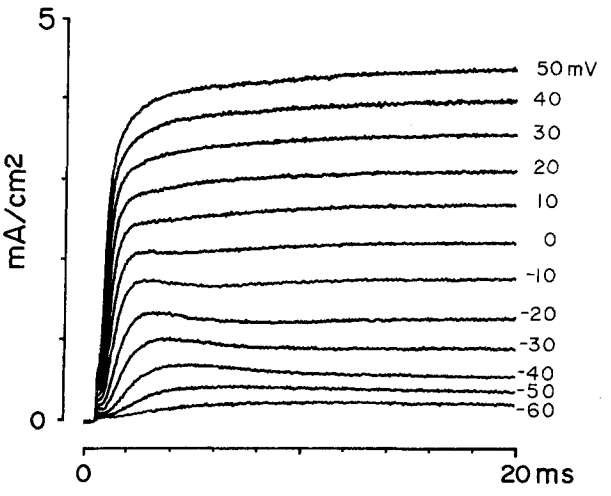

Fig. 2. Outward currents uncorrected for leakage rectification. Experiment 790618C: fiber in ASW plus TTX at 18 °C. Cut ends of the fiber in solution KF-1. The holding potential was estimated from the $h_\infty - V$ curve for the sodium current at -100 mV. Absolute membrane potential during the pulses is given next to each record

tions were designed to test the possibility that the outward current is generated in more than one conductance system as suggested before (Connor, 1975; Connor et al., 1977).

Potassium Ions Possible Carriers of the Outward Currents

Three experimental results strongly suggest that the outward currents shown in Fig. 3 are carried by potassium ions. Internal application of Cs^+ reduced the outward currents. In the preceding work we have seen that when the ends of the fiber were cut in a solution with Cs^+ the outward currents were completely eliminated from the records.

In other experiments we cut the fibers in solutions with various concentrations of Na^+. We always measured a decrease in the size of the outward currents, confirming previous observations (Bezanilla & Armstrong, 1972). One example of these effects of

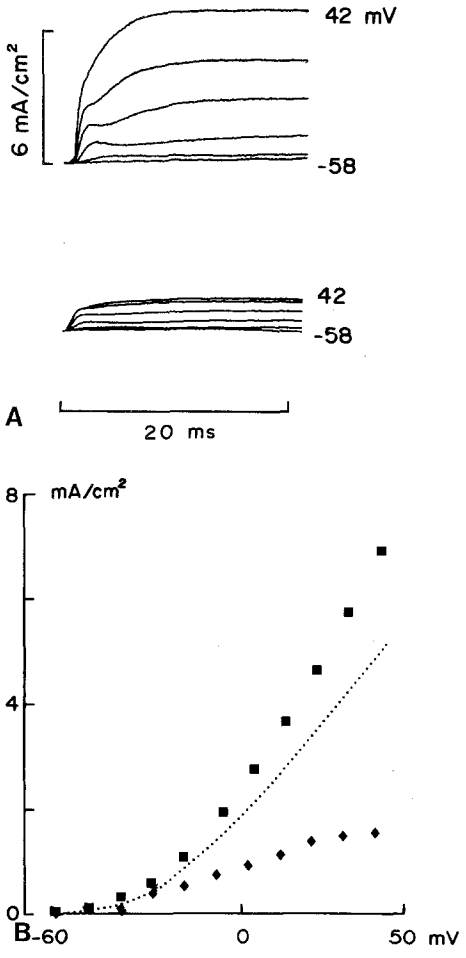

Fig. 3. Effects of internal application of Na^+ on outward currents. **A:** Membrane currents recorded in ASW plus TTX and KF-1 in pools *C* and *E* (*upper part*). Shown in the lower part are the membrane current records 10 min after the application of 150 mM Na^+ (solution KF/NaF). Potential during the pulses (increased in 20-mV steps) is given for the first and last record in the series. **B:** Current-voltage curves calculated from the records in part *A*. ■ with KF-1 and ◆ with KF/NaF. Dashed curve represents I' and was calculated from the values measured in KF-1, namely I, using the independence principle corrections as follows:

$$I' = \frac{\alpha|Na^+|'_o - (\alpha|Na^+|'_i + |K^+|'_i)\exp(FV/RT)}{\alpha|Na^+|_o - |K^+|_i \exp(FV/RT)} \times 1$$

where F, R and T have their usual meaning ($RT/F = 24.5$ mV). α represents the selectivity ratio P_{Na}/P_K taken as 0.002. | | represents the chemical activity of the cations measured with cation-sensitive electrodes. Experiment 790620: holding potential −98 mV; temperature 19 °C

internal application of Na^+ is illustrated in Fig. 3. Shown in part *A* are the outward current records made with the cut ends of the fiber in solution KF-1 (upper part) and, 10 min after the replacement of the solution in pools *C* and *E* by solution KF/NaF (lower part). The $I-V$ curves shown in part *B*, namely ■ in KF-1 and ◆ in KF/NaF, were measured at 20 msec. The dotted curve was calculated from

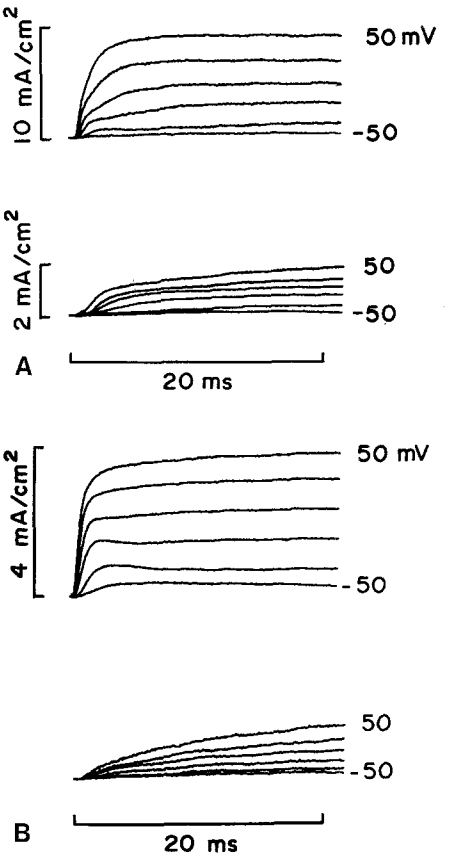

Fig. 4. Effects of internal application of TEA and effects of external application of 4-AP on outward currents. **A:** outward currents recorded in ASW plus TTX with KF-1 in pools *C* and *E* (upper part) and 10 min after the addition of TEA at a concentration of 5 mM. Experiment 790618C: holding potential, −100 mV; temperature 18 °C. **B:** membrane currents recorded in ASW plus TTX with KF-1 in pools *C* and *E* (upper part) and 5 min after the addition of 20 mM 4-AP to the external medium. Experiment 790618B: holding potential, −100 mV; temperature 12 °C

the values measured in KF-1 using the equation given in the legend to Fig. 3 taken from Binstock and Lecar (1969).

Internal application of tetraethylammonium (TEA) by diffusion from pools *C* and *E* along the axoplasm also blocks the outward currents. Furthermore, another specific blocker of K^+ channels, 4 amino-pyridine (4-AP) blocks both components of the outward currents when applied either externally or internally. These effects are illustrated in Fig. 4. Shown in part *A* are two sets of outward currents recorded in ASW plus TTX, the records in the upper part with the cut ends of the fiber in KF-1 and the records in the lower part in KF-1 plus TEA. Figure 4*B* demonstrates the blocking effect of 4-AP.

As in most of the experiments considered in this paper K^+ was the main cation present inside the

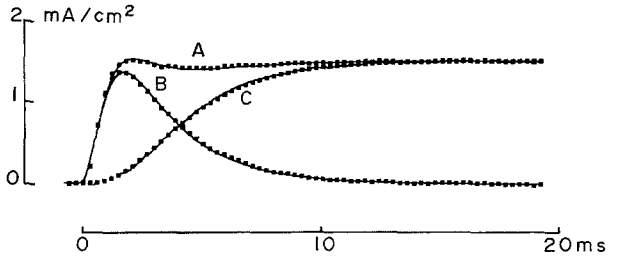

Fig. 5. Analysis of the total outward current *A* into components *B* and *C*. Experiment 790618A: fiber in ASW plus TTX at 18 °C. Cut ends in solution KF-1. (*A*) Outward current in response to a sudden displacement in membrane potential from −120 to −10 mV. To acquire this record a sampling rate of 100,000 Hz was used. Each point represents the average of 30 samples. (*B*, *C*) The points were derived from *A* as explained in the text. The curve was calculated with the term in Eq. (3) representing i_{K_1} for *B* and representing i_{K_2} for *C*. It represents the best fit to the points

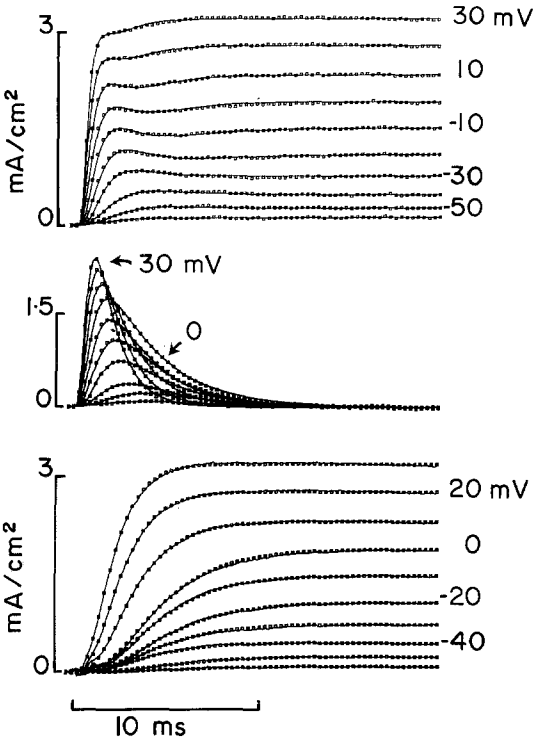

Fig. 6. Analysis of the total outward currents into two components. Experiment 790618A: Fiber in ASW plus TTX at 18 °C. Internal solution KF-1. $V_h = -120$ mV. Absolute membrane potential during pulses is indicated next to the records. *Top*: Symbols represent total outward current, average of 30 samples taken every 10 µsec. Solid line was calculated with Eq. (3). *Middle*: Component with activation-inactivation kinetics. Solid line was calculated with the term representing i_{K_1} in Eq. (3). *Bottom*: Component with activation kinetics only. Solid line was calculated with the term representing i_{K_2} in Eq. (3)

fibers, it seems quite likely that both components of the outward currents are carried by K^+. Hereafter they will be called i_{K_1} and i_{K_2}.

Two Possible Components in the Outward Current Records

Figure 5 illustrates the analysis of one current record (*A*) into two components, namely, an early component with activation-inactivation kinetics (*B*) and a delayed component with activation kinetics only (*C*).

This analysis is based on the idea that crustacean repetitive nerve fibers have two potassium conductance systems (Connor et al., 1977). The early component can be described using the m^3h Hodgkin-Huxley formalism and the delayed component using the n^4 description (Hodgkin & Huxley, 1952*b*).

We may write

$$g_{K_1} = \bar{g}_{K_1} n_1^3 h_K \tag{1}$$

$$g_{K_2} = \bar{g}_{K_2} n_2^4 \tag{2}$$

where $\bar{g}_{K_1}$, $\bar{g}_{K_2}$ represent maximum conductances for a given membrane potential, n_1, h_K and n_2 are the state variables defined as the *m*, *h* and *n* variables in the Hodgkin-Huxley system.

The total potassium current, namely $i_{K_1} + i_{K_2}$, should be represented by the equation

$$i_K = i_{K_1,\max}(1-\exp(-(t-\delta t/\tau_{n_1})^3 \cdot \exp(t/\tau_{h_K}) + i_{K_2,\max}(1-\exp(-t/\tau_{n_2}))^4 \tag{3}$$

where τ_{n_1} and τ_{n_2} represent the time constants for the activation of i_{K_1} and i_{K_2}, respectively, τ_{h_K} represents the time constant of inactivation of i_{K_1} and δt represents a delay in the start of the early potassium conductance change.

At 18 °C I_K records reached steady level in about 20 msec. In practice, therefore, the last 5 msec of each record in Fig. 5 can be considered to represent i_{K_2}. This part of the record was used to determine the steady level of i_{K_2} and τ_{n_2}. This was done by fitting the tail end of the function n^4 to the last points in each record. The complete time course of this component was then calculated and subtracted from the current record to give i_{K_1}. The resulting difference (measured outward current minus $i_{K_2,\max}((1-\exp(-t/\tau_{n_2}))^4)$ was fitted as described by Keynes and Rojas (1976) in the case of sodium currents. The $i_{K_1,\max}$, $i_{K_2,\max}$, τ_{n_1}, τ_{n_2}, τ_{h_K} and δt values obtained were used to calculate, using Eq. (3), the solid lines in Fig. 5, 6 and 11.

The goodness of the fit, a measure of the validity of the present analysis, was evaluated using a computer program designed to minimize the following residual,

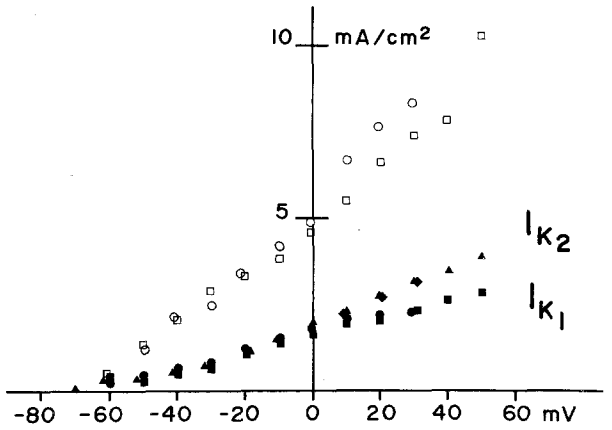

Fig. 7. Current-voltage relationships. Maximum values for i_{K_1} and i_{K_2} were obtained as illustrated in Fig. 6. Experiments 790618A (■, ◆) and 790618C (●, ▲). To calculate the $i_{K_1}-V$ curve corrected for inactivation (□, ○) the $i_{K_1}(t)$ component (obtained as illustrated in Fig. 6) was divided by $\exp(-t/\tau_{h_K})$. Temperature for both experiments: 18 °C

Table 2. Maximum potassium conductances

(a) Experiment	(b) V_h (mV)	(c) g_{K_1} (mmho/cm²)	(d) $g^*_{K_1}$ (mmho/cm²)	(e) g_{K_2} (mmho/cm²)	Temp. (°C)
790618A	−120	21	78	29	18
790618B	−100	20	65	28	12
790618C	−100	22	80	30	18

All experiments in this Table were done using the Dodge-Frankenhaeuser feedback system. Experiments 790618B and 790618C were corrected for leakage conductance. For g_{K_2}, 20-msec pulses were used. For $g^*_{K_1}$ the I_{K_1} records were first analyzed using $n_1^3 h_K$-kinetics and then corrected for inactivation h_K.

$$\left[\frac{\sum_{k=1}^{N}(I_k-i_k)^2}{N}\right]^{\frac{1}{2}}$$

where i_k is the fitted value and I_k is the measured current (*see* next section). The fit illustrated in Fig. 5 remains satisfactory when other records at different membrane potentials were considered. This is clearly seen in Fig. 6 where a set of outward current records (upper part of Fig. 6) at membrane potentials in the range of −60 to 30 mV were analyzed as described in Fig. 5.

Shown in Fig. 7 are the steady-state values of the currents i_{K_1} and i_{K_2}. Assuming that these currents flow through two different, noninteracting channels, one can calculate the size of i_{K_1}, if there were no inactivation. These values are also plotted in Fig. 7. Maximum chord conductance values calculated from these current-voltage relations are given in Table 2.

Kinetics and Steady-State Characteristics of the Two Potassium Systems

Table 3 summarizes the data obtained from the analysis of the outward currents as presented in Fig. 6. The values of the time constants for the activation and inactivation of i_{K_1} are given in columns (b) and (c). The time constant for the activation of i_{K_2} is under column (f). It should be noted that τ_{h_K} is rather similar to τ_{n_2}. On the other hand, the time constant for the inactivation of the sodium conductance (*see* preceding paper) is one order of magnitude smaller than either τ_{h_K} or τ_{n_2}.

From the two-state transition model (Hodgkin & Huxley, 1952*b*) one can define the time constants as

$$\tau_{n_i}=\frac{1}{\alpha_{n_i}+\beta_{n_i}} \tag{4a}$$

and the fraction in open configuration in the steady state as

$$n_{i,\infty}=\frac{\alpha_{n_i}}{\alpha_{n_i}+\beta_{n_i}} \tag{4b}$$

where $i=1, 2$. $n_{i,\infty}$ values were calculated from the $I-V$ curves with i_{K_1} corrected for inactivation for $n_{1,\infty}$ and i_{K_2} measured either at 30 or at 60 msec. The chord conductance values were calculated first and then, the $n_{i,\infty}$ values were calculated with Eqs. (1) and (2). With the fibers in ASW (11 mM $[K^+]_o$) the instantaneous $I-V$ curve is linear in the membrane potential range from −60 to 60 mV (Quinta-Ferreira, 1981). Therefore, it is safe to assume that within that potential range both $n_{i,\infty}$ values are accurately estimated. Eq. (4a, b) were resolved for α_{n_i} and β_{n_i}. Shown in the upper part of Fig. 8 are the values of the rate constants and, in the lower part, the values of the time constants. The curves in the upper part of Fig. 8 represent the best fit to the points and were calculated using linear-exponential rate functions of the form:

$$\alpha_{n_i}=1000(A_i+B_iV)/(1-\exp C_i(A_i+B_iV)) \tag{5a}$$

$$\beta_{n_i}=1000(a_i+b_iV)(\exp c_i(a_i+b_iV)-1). \tag{5b}$$

The lower part of Fig. 8 shows the experimental values of τ_{n_1} and τ_{n_2} and the calculated curves.

The steady-state n_1 and n_2 functions are presented in Fig. 9. $n_{1,\infty}$ equals 0.5 at −71 mV and $n_{2,\infty}$ equals 0.5 at −67 mV. While 17.5 mV induced an *e*-fold change in $n_{1,\infty}$ at −71 mV, 33.5 mV induced the same change in $n_{2,\infty}$.

Effects of Membrane Potential on i_{K_1} and i_{K_2}

The data in Table 3 (column (c)) suggests that for membrane potentials in the range from −60 to

Table 3. Kinetics and steady-state parameters for the outward current components

Exp No.	(a) V_M	(b) i_{K_1}	(c)	(d)	(e)	(f) i_{K_2}	(g)	V_h	Temp.
	(mV)	τ_{n_1} (msec)	τ_{h_K} (msec)	$I_{K_1,peak}$ (mA/cm^2)	$I_{K_1,max}$ (mA/cm^2)	τ_{n_2} (msec)	$I_{K_2,max}$ (mA/cm^2)	(mV)	
790618A	−60	2.31	3.62	0.09	0.40	3.75	0.10	−120	18
	−50	2.10	3.22	0.21	1.12	3.16	0.25		
	−40	1.57	2.57	0.36	2.04	2.24	0.46		
	−30	1.02	2.81	0.71	2.39	2.54	0.75		
	−20	1.01	2.64	1.05	3.46	2.70	1.08		
	−10	0.82	2.46	1.36	4.00	2.44	1.50		
	0	0.59	2.74	1.70	4.78	2.37	1.91		
	+10	0.65	1.79	1.92	6.56	1.73	2.33		
	+20	0.58	1.40	2.13	7.37	1.36	2.80		
	+30	0.50	1.15	2.32	8.60	1.11	3.22		
790618B	−30	1.05	1.92	0.31	1.64	1.86	0.47	−100	12
	−20	0.74	2.68	0.58	1.89	2.38	0.62		
	−10	0.73	1.39	0.75	3.97	1.49	0.96		
	0	0.57	1.41	0.97	4.08	1.50	1.22		
	10	0.68	0.99	1.15	8.00	1.28	1.60		
	20	0.60	1.08	1.45	7.28	1.32	1.96		
	30	0.51	1.34	1.70	5.67	1.36	2.31		
	40	0.60	1.33	1.95	6.70	1.35	2.69		
	50	0.49	1.47	2.25	6.61	1.37	3.08		
790618C	−60	2.59	5.02	0.15	0.53	4.15	0.22	−100	18
	−50	2.15	3.86	0.30	1.35	3.50	0.35		
	−40	1.59	3.43	0.51	2.09	3.18	0.48		
	−30	1.30	2.32	0.72	3.48	2.36	0.80		
	−20	0.90	4.91	1.11	2.24	3.95	1.08		
	−10	0.64	3.93	1.43	3.06	3.13	1.55		
	0	0.73	3.68	1.71	3.56	2.86	1.95		
	10	0.79	2.85	1.95	5.50	2.47	2.38		
	20	0.79	1.82	2.05	6.69	1.72	2.74		
790620A	−28	0.96	6.05	0.59	1.17	5.41	0.49	−98	19
	−18	1.01	3.10	0.86	2.68	3.74	1.04		
	−8	0.91	1.83	1.67	6.71	2.93	1.92		
	2	0.86	1.87	1.47	6.40	2.56	2.71		
	12	0.52	2.32	1.86	5.12	2.30	3.63		
790620B	−25	1.00	5.48	4.66	10.19	4.62	4.70	−105	19
	−15	1.06	4.11	6.53	15.87	3.76	7.90		
	−5	0.78	3.14	8.07	20.50	2.93	11.01		
	+5	0.75	4.09	10.34	22.11	3.17	14.38		
790620C	−25	1.79	4.49	1.25	–	3.96	3.01	−65	19
	−15	1.30	3.82	1.63	–	3.21	5.58		
	−5	1.98	3.09	2.88	–	3.03	8.34		
	+5	2.34	2.09	3.45	–	2.49	11.54		

Data obtained with the Dodge and Frankenhaeuser feedback amplifier system. Data corrected for leakage in experiments 790618B (g_L = 5.3 mmho/cm^2), 79618C (g_L = 5.2 mmho/cm^2) and 790620A (g_L = 60 mmho/cm^2). g_L = 0 in the other experiments. In experiments performed at temperatures different from 18 °C, time constants were corrected for these temperatures assuming a Q_{10} of 3.

50 mV, the process of inactivation of i_{K_1} is completed in about 10 msec at 18 °C. In order to characterize the time course of this inactivation we performed standard double-pulse experiments (Hodgkin & Huxley, 1952*a*; Quinta-Ferreira et al., 1982). The results of one such experiment are illustrated in Fig. 10 (only the time course of inactivation at three membrane potentials are shown). For this experiment the duration of V_1 was increased from 0.8 to 102 msec. The initial values for n_1 and n_2 were estimated from Fig. 6 and 9. The two components were separated as explained in Fig. 5. The maximum value of i_{K_1} measured when V_1 was set at 0.8 msec was used to normalize the maximum values obtained with longer V_1 pulses. The time constants of inactivation were obtained from the fit of a single time

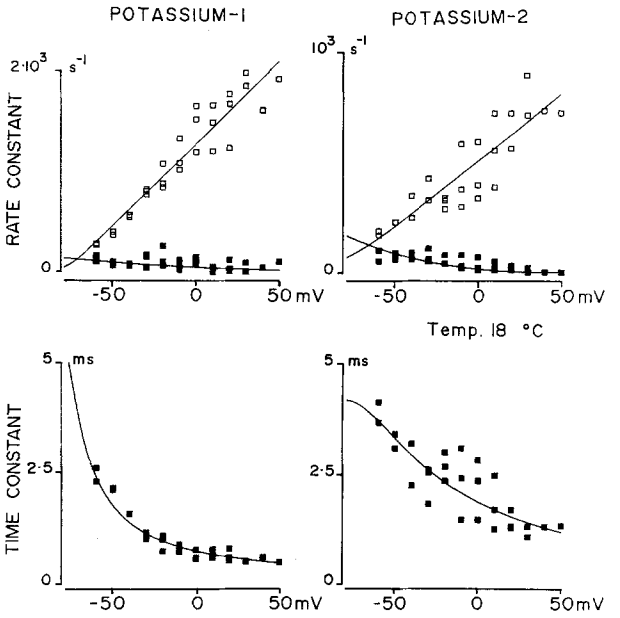

Fig. 8. Activation rate and time constants for g_{K_1} and g_{K_2}. Experiments: 790618A at $V_h = -120$ mV and 18 °C; 790618B at $V_h = -100$ mV and 12 °C; 790618C at $V_h = -100$ mV and 18 °C. The rate constants for experiment at 12 °C were adjusted to 18 °C assuming $Q_{10} = 3$. *Left side, upper figure:* $\square\alpha_{n_1}$, $\blacksquare\beta_{n_1}$; *lower figure:* $\blacksquare\tau_{n_1}$. *Right side, upper figure:* $\square\alpha_{n_2}$, $\blacksquare\beta_{n_2}$; *lower figure:* $\blacksquare\tau_{n_2}$. Continuous lines represent the least-squares regression curves calculated using equations given in the text. The following coefficients were used for i_{K_1}: $A = 1.29$, $B = 0.016$, $C = -20.0$, $a = 0.077$, $b = -0.00059$, $c = 6.0$; and for i_{K_2}: $A = 0.51$, $B = 0.006$, $C = -20.0$, $a = 0.036$, $b = -0.0008$, $c = 10.0$

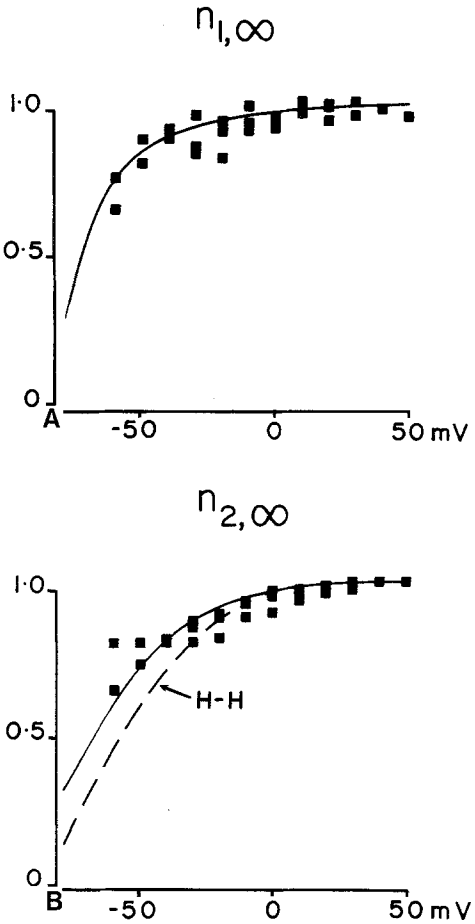

Fig. 9. $n_{1,\infty}$ and $n_{2,\infty}$ values as a function of membrane potential. Same experiments as for Fig. 6. $n_{1,\infty} = 0.5$ at $V = -71$ mV. $n_{2,\infty} = 0.5$ at $V = -67$ mV. Curves were calculated as $n_{1,\infty} = \frac{\alpha_{n_1}}{\alpha_{n_1} + \beta_{n_1}}$, $n_{2,\infty} = \frac{\alpha_{n_2}}{\alpha_{n_2} + \beta_{n_2}}$ where $\alpha_n = 1{,}000(A + BV)/(1 - \exp C(A + BV))$, $\beta_n = 1{,}000(a + bV)(\exp c(a + bV) - 1)$ with parameters as follows: $A = 1.291$, $B = 0.016\ \text{mV}^{-1}$, $C = -20.0$, $a = 0.077$, $b = -0.0006\ \text{mV}^{-1}$, $c = 6.0$ for n_1 and $A = 0.511$, $B = 0.006\ \text{mV}^{-1}$, $C = -20.0$, $a = 0.036$, $b = -0.0008\ \text{mV}^{-1}$, $c = 10.0$ for n_2

constant to the experimental values. For the prepulse membrane potentials at −60, −50 and −40 mV the time constants τ_{h_K} obtained in this experiment were 15.1, 8.4 and 7.2 msec, respectively. The average time constants measured at the same potentials given in Table 3 under column (c) are 4.32, 3.54 and 3.0 msec.

If we allow for the temperature difference and assume a temperature coefficient Q_{10} of 3, the corresponding values in Fig. 10 decrease to 11.6, 6.5 and 5.5 msec, respectively. The two sets of values are different.

One possible explanation for this discrepancy may be related to the initial delay in the start of the potassium inactivation in Fig. 10. Thus, it may be seen in Fig. 10 that at $V_1 = -60$ mV the points started to decrease with the point at 1.0 msec.

On the other hand, as the time course of the inactivation shown in Fig. 10*B* is affected by the size of the peak of i_{K_1} estimated from the analysis of the total current into i_{K_1} plus i_{K_2}, small changes in $\tau_{n_{K_2}}$ greatly affect the τ_{hK} values and, therefore the estimated maximum i_K required to calculate the time course shown in Fig. 10*A*. This is shown on the left side. Taking $\tau_{n_2} = 2.79$ msec gave $\tau_{n_1} = 0.805$ msec, $\tau_{h_K} = 2.62$ msec and a peak value for i_{K_1} equal to 2.463 mA/cm². The residual of the fit was 0.027 μA/cm². Taking $\tau_{n_2} = 2.46$ msec gave $\tau_{n_1} = 1.08$ msec, $\tau_{h_K} = 1.04$ msec and the peak value of i_{K_1} decreased to 1.63 mA/cm². The residual of the fit was 0.072 μA/cm² (2.7 times larger than in the previous fit). The first set of time constants was kept unchanged for the analysis of the records which were used to calculate the time course of the inactivation shown in Fig. 10*B* (the residual from each fit was smaller than 2.8×10^{-3} mA/cm²). If the second set of time constants is used instead and they are kept unchanged, the time course of the inactivation is practically unaffected.

Although it seems that the initial delay in the

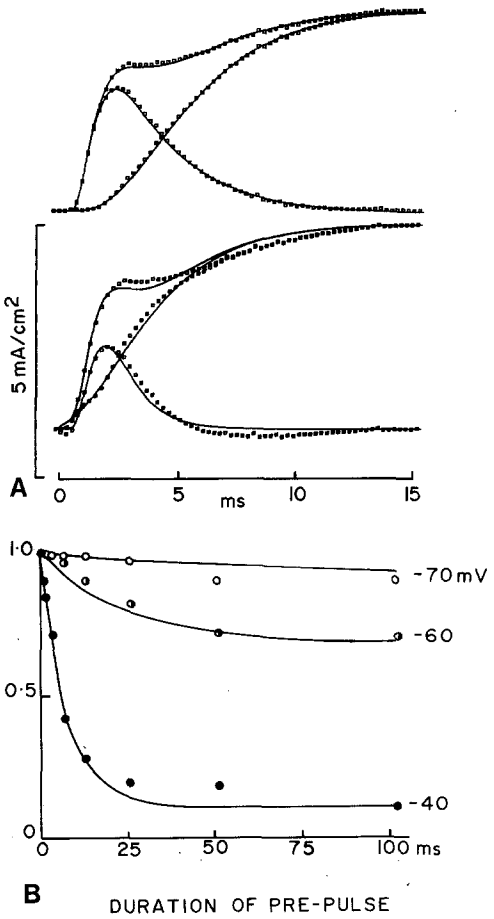

Fig. 10. Development of the inactivation of i_{K_1} at various membrane potentials. Experiment 800421: fiber in ASW plus TTX at 15.6 °C. Cut ends in KF-1. Holding potential set at −120 mV. **A:** Analysis of the total current into two components and the effects of changing τ_{h_K} from 2.62 (upper set of curves) to 1.04 msec (lower set of curves). **B:** Analysis of the time course of the development of the fast inactivation of i_{K_1}. Prepulse durations for each series (with V_1 set as indicated next to each time sequence) were tp = 0.8, 1.6, 3.2, 6.4, 12.8, 25.6, 51.2 and 102.4 msec. Vertical axis represents $i_{K_1,max}(V_1, tp)/i_{K_1,max}(V_1, 0.8)$

start of the inactivation causes the discrepancy, the curves in Fig. 10*B* should be taken as rough indications of the time course of the inactivation.

The dependence on membrane potential of the inactivation processes was measured by changing V_1 with its duration set at 102 msec. The results of one experiment are illustrated in Fig. 11. The curves on the upper part represent the analysis of the outward current in response to a test pulse to −20 mV from a holding potential of −120 mV. The lower part represents the fraction of K_1 or K_2 channels available to conduct current as a function of the membrane potential during V_1. The curves represent a least-squares fit of $h_{K_1,\infty}$ and $h_{K_2,\infty}$ functions calculated as

$$h_{K_1,\infty} = \frac{1}{1+\exp(A_1 + B_1 V_1)} \tag{6a}$$

$$h_{K_2,\infty} = \frac{1}{1+\exp(A_2 + B_2 V_1)}. \tag{6b}$$

At $V_1 = -70$ mV a 27.9 mV change in potential corresponds to an e-fold change in $h_{K_1,\infty}$, but a 231.3 mV change in potential is required in the case of $h_{K_2,\infty}$. It should be noticed that for V_1 values more positive than −60 mV, the observed reduction in i_{K_2} is likely to be in part due to accumulation of K^+ in the spaces between the axolemma and the Schwann cells (Quinta-Ferreira, 1981).

To be able to measure the true time course of the potassium conductance with the fiber in artificial seawater, it is necessary to evaluate the changes in V_K as a function of time due to the accumulation of K^+ in the extracellular space (Frankenhaeuser & Hodgkin, 1956).

Comparison of the Time Constants for Turning off the Potassium Conductance

One way to minimize the effects of the accumulation of K^+ discussed in the preceding section is to carry out the experiments in Na-free, high K^+-seawater.

Shown in Fig. 12 are two sets of potassium current records made in high K^+-seawater plus 300 nM TTX. As the holding potential is −108 mV negative to the K^+ equilibrium potential, small depolarizations induce inward K^+ currents. It is also clear that the inward current tails reach the holding current level in less than 15 msec, suggesting that the K^+ conductance is turned off in that time.

Figure 13 shows the analysis of the current tails obtained in high K^+-seawater. The current tails recorded after 4.8-msec pulses are presented on the lower left part and those recorded after 29.5-msec pulses on the lower right part. While the tail currents after 4.8 msec could be described as the sum of two exponentials, only one exponential fitted perfectly well the time course of the tails after 29.5-msec pulses. Furthermore, the ratio $i_{K_1}(0) + i_{K_2}(0)$ after 4.8-msec pulses/$i_{K_2}(0)$ after 29.5-msec pulses is constant at 1.06 ± 0.11. The values of the ratio $i_{K_2}(0)/i_{K_1}(0)$ after 4.8-msec pulses are 6.9 (after a pulse to 2 mV), 5.7, 3.8, 5.0 and 12.2 (after a pulse to 82 mV). The analysis shown in Fig. 6 was repeated for the records at 2, 22, 42 and 82 mV not shown in Fig. 13. The i_{K_2}(4.8 msec)/i_{K_1}(4.8 msec) ratios are 1.2 (pulse to 2 mV), 1.6, 3.4, 6.0 and 19.0 (pulse to 82 mV).

Since the time constants for turning off the potassium conductance at the end of a depolarizing pulse, $\tau_{off,1}$ and $\tau_{off,2}$ were measured at a constant

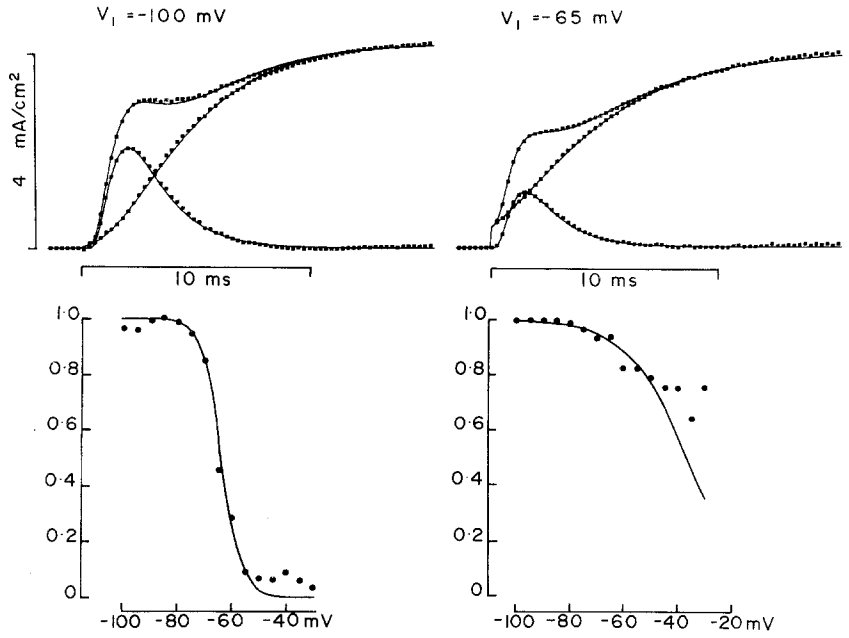

Fig. 11. Effects of membrane potential on i_{K_1} and i_{K_2}. Experiment 800421: fiber in ASW plus TTX at 15.6 °C. Cut ends in 500 mM KF. Sampling rate was 25,000 Hz. Each point represents the average of six samples. The prepulse V_1 duration was 102 msec. *Upper part:* separation of i_{K_1} and i_{K_2} from the measured outward current. *Lower part:* vertical axis represents $i_K(V_1, V_2)/i_K(V_1 = V_h, V_2)$ for component i_{K_1} (left side) and component i_{K_2} (right side). Absolute membrane potential during test pulse was 0 mV. Curves calculated as described in the text with $A_1 = 17.0$, $B_1 = 0.267\ \text{mV}^{-1}$ for $h_{K_1,\infty}$. $A_2 = 3.3$, $B_2 = 0.091\ \text{mV}^{-1}$ for $h_{K_2,\infty}$

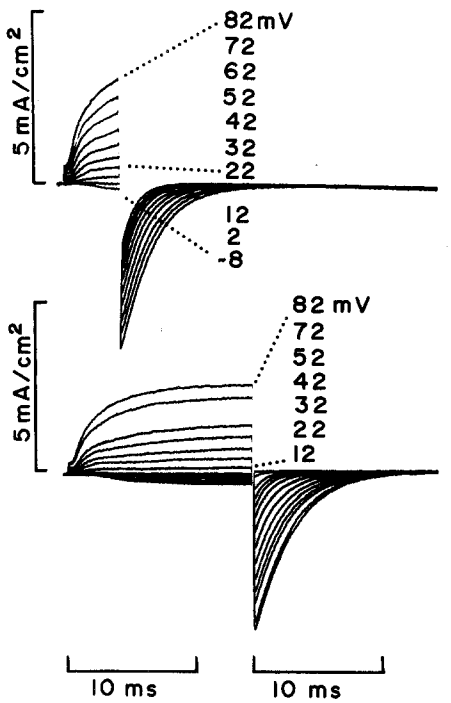

Fig. 12. Potassium currents in high K^+ seawater. Experiment 810211: fiber in high K^+-SW at 12.5 °C. Cut ends in KF-1. Holding potential set at −108 mV. Absolute membrane potentials during the test pulses are given next to the corresponding current trace

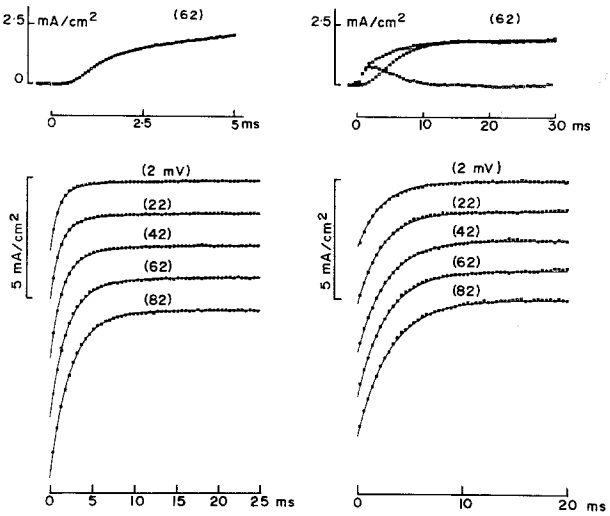

Fig. 13. Time constants determining the decline of potassium currents following repolarization. Experimental conditions as for experiment in Fig. 12. Symbols represent samples of potassium currents. The curve represents the least-squares fit of either two exponential functions (*left side*) or one exponential function to the points. Time constants as follows:

	Tails after 4.8 msec				after 29.5 msec	
Vp (mV)	$i_{K_1}(0)$ (mA/cm^2)	$i_{K_2}(0)$ (mA/cm^2)	$\tau_{off,1}$ (msec)	$\tau_{off,2}$ (msec)	$i_{K_2}(0)$ (mA/cm^2)	τ_{off} (msec)
2	0.36	2.49	5.4	0.9	2.75	2.3
22	0.53	3.02	4.5	1.1	3.82	2.4
42	0.98	3.73	3.9	1.3	4.70	2.7
62	0.98	4.88	4.4	1.8	5.33	2.7
82	0.53	6.48	4.6	2.3	5.68	3.1
Avg. ± SD			4.56 ± 0.54	1.48 ± 0.57		2.64 ± 0.31

holding potential of −108 mV we can take the average values from Fig. 13 as $\tau_{off,1} = 4.56 \pm 0.54$ msec and $\tau_{off,2} = 1.48 \pm 0.57$ msec at the end of a 4.8 msec depolarizing pulse and, $\tau_{off,1} = 2.64 \pm 0.31$ at the end of the 29.8-msec pulse.

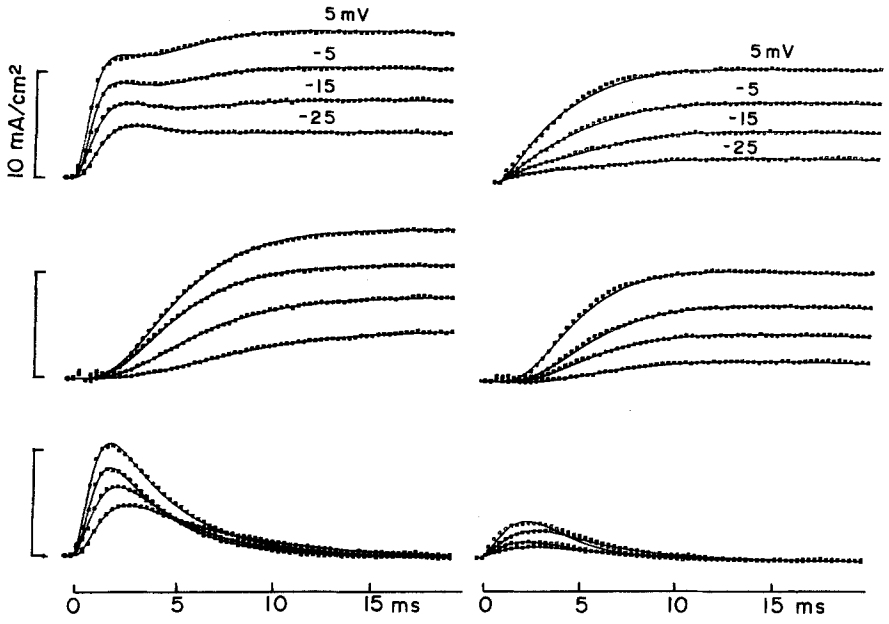

Fig. 14. Effects of membrane potential on i_{K_1} and i_{K_2}. Experiment 790620: fiber in ASW plus TTX. Cut ends of the fiber in KF-1 at pH 7.4. The membrane potential during the pulses for the six sets of current records are indicated in mV on the right side, next to the current records representing I_{K_2}. Temperature: 19 °C

The Hodgkin-Huxley type time constants can be calculated from the τ_{off} values and are $\tau_{n_1} = 13.7\,\text{msec}(4.56 \times 3)$, $\tau_{n_2} = 5.9\,\text{msec}(1.48 \times 4)$ for the 4.8 msec pulse and $\tau_{n_2} = 10.6\,\text{msec}(2.64 \times 4)$ for the 29.8 msec pulse. Corresponding τ_{n_1} and τ_{n_2} values can be calculated from the empirical equations used to fit the experimental points in Fig. 8 and are $\tau_{n_1} = 5.26\,\text{msec}$ and $\tau_{n_2} = 3.30\,\text{msec}$ at $-108\,\text{mV}$. Allowing for the temperature difference (18 °C for the curve in Fig. 8 and 12.5 °C for Fig. 13), assuming a Q_{10} of 3, the corrected values are $\tau_{n_1} = 9.5$ and $\tau_{n_2} = 5.9\,\text{msec}$. These values are smaller than the measured 13.7 and 8.2 msec ($=(5.9+10.6)/2$). These results are in agreement with Swenson and Armstrong (1981) who reported recently that in squid giant axons, potassium channels close more slowly in the presence of high external K^+ as for the experiments in Figs. 12 and 13.

Effects of Holding the Membrane Potential at −65 mV

The results presented using the double-pulse procedure suggest that both potassium systems can be inactivated by membrane depolarization. However, in order to test the possibility of an ultraslow inactivation with time constants in the range of minutes affecting the gating structures in these channels, it is necessary to maintain the membrane depolarized during seconds (Ehrenstein & Gilbert, 1966). Figure 14 illustrates the results of one experiment in which for the control run the membrane was held at −105 mV. The records shown on the left side (−105 mV) can be compared with the records obtained from a holding potential of −65 mV shown on the right. The potential during the pulse is indicated next to the records. From the maximum values for i_{K_1} and i_{K_2} we estimate h_{K_1} and h_{K_2} at −65 mV as 0.31 and 0.71, respectively. The corresponding values from Fig. 11 are 0.50 and 0.93. However, these differences are not statistically significant.

It seems, therefore, that i_{K_1} exhibits fast inactivation and that the ultra slow inactivation seen in the giant axon of the squid (Ehrenstein & Gilbert, 1966) is not present in these fibers.

Discussion

The analysis of the outward current records in terms of two components with different kinetics presented here strongly supports the idea that the potassium system in these nerve fibers is different from that in the giant axon of the squid (Hodgkin & Huxley, 1952*a*). To account for the observed kinetics we have used the Hodgkin-Huxley concept that the gates undergo first order transitions between two energy configurations. The underlying hypotheses in the analysis are three: *i*) There are two different, noninteracting potassium channels, *ii*) the gates undergo first-order transitions leading to the opening and closing of the potassium channels and, *iii*) while to open a K_1 channel three gates have to undergo the transition to the activated state (four gates in the case of the K_2 channel), only one gate has to return to the resting configuration to turn off the potassium current in that channel. In the case of i_{K_1} the

conductance state of the channel is also affected by the state of the inactivation gate.

It is also possible to account for the observed kinetics assuming a higher order transition of the gates along a series of energy configurations.

Although until we find specific blockers for these postulated conductance systems, our analysis must be considered as a working hypothesis, we would like to give arguments in favor of the idea of different gating structures for K_1 and K_2.

The most important argument in support of this hypothesis is provided by the excellent fit of the total outward currents illustrated in Fig. 6.

The effects of membrane potential on K_1 and K_2 illustrated in Figs. 9, 11 and 14 demonstrate that the voltage sensitivity of the activation gates and of the inactivation gates is fundamentally different, for these curves have different mid-point potentials and different slopes.

Another argument in support of this hypothesis is provided by the analysis of the time course of the potassium currents illustrated in Fig. 13. Two time constants are required to fit tails when both i_{K_1} and i_{K_2} have been activated during the test pulse and only one time constant is required when i_{K_1} is fully inactivated and only i_{K_2} remains.

This research was supported by the Science Research Council. It was submitted by Emilia Quinta-Ferreira as part of a Ph.D. thesis for the School of Biological Sciences, University of East Anglia. During this work Emilia Quinta-Ferraira was supported by the Calouste Gulbenkian Foundation. The secretarial assistance of Mrs. S. Garrod is acknowledged.

References

Arispe, N., Quinta-Ferreira, M.E., Rojas, E. 1980. Two potassium conductance systems in the giant axon of the crab *Carcinus maenas*. *J. Physiol.* (*London*) **305**:87P–88P

Bezanilla, F., Armstrong, C.M. 1972. Negative conductance caused by entry of sodium and caesium ions into the potassium channels of squid axons. *J. Gen. Physiol.* **60**:588–608

Binstock, L., Lecar, H. 1969. Ammonium ion currents in the squid giant axon. *J. Gen. Physiol.* **53**:342–361

Connor, J.A. 1975. Neural repetitive firing: A comparative study of membrane properties of crustacean walking leg axons. *J. Neurophysiol.* **38**:922–932

Connor, J.A., Walter, D., McKown, R. 1977. Neural repetitive firing. Modifications of the Hodgkin-Huxley axon suggested by experimental results from crustacean axons. *Biophys. J.* **18**:81–102

Dodge, F.A., Frankenhaeuser, B. 1958. Membrane currents in isolated frog nerve fibre under voltage clamp conditions. *J. Physiol.* (*London*) **143**:76–90

Ehrenstein, G., Gilbert, D.L. 1966. Slow changes in potassium permeability in squid giant axon. *Biophys. J.* **6**:553–566

Frankenhaeuser, B., Hodgkin, A.L. 1956. The after-effects of impulses in the giant nerve fibres of *Loligo*. *J. Physiol.* (*London*) **131**:341–376

Hodgkin, A.L., Huxley, A.F. 1952*a*. The dual effect of membrane potential on sodium conductance in the giant axon of *Loligo*. *J. Physiol.* (*London*) **116**:497–506

Hodgkin, A.L., Huxley, A.F. 1952*b*. A quantitative description of membrane current and its application to conduction and excitation in nerve. *J. Physiol.* (*London*) **117**:500–544

Hodgkin, A.L., Huxley, A.F., Katz, B. 1952. Measurement of current-voltage relations in the membrane of the giant axon of *Loligo*. *J. Physiol.* (*London*) **116**:424–448

Keynes, R.D., Rojas, E. 1976. The temporal and steady-state relationships between activation of the sodium conductance and movement of the gating particles in the squid giant axon. *J. Physiol.* (*London*) **255**:157–189

Quinta-Ferreira, M.E. 1981. Ionic channels in the giant axon of the crab *Carcinus maenas*. Ph.D. Thesis. School of Biological Sciences, University of East Anglia, Norwich

Quinta-Ferreira, M.E., Arispe, N., Rojas, E. 1982. Sodium currents in the giant axon of the crab *Carcinus maenas*. *J. Membrane Biol.* **66**:159–169

Swenson, R.P., Jr., Armstrong, C.M. 1981. K^+ channels close more slowly in the presence of external K^+ and Rb^+. *Nature* (*London*) **291**:427–429

Received 5 March 1981; revised 10 July 1981